Computers, Materials & Continua
DOI:10.32604/cmc.2020.013946
Article

Tech Science Press

Hybrid Metamodel—NSGA-III—EDAS Based Optimal Design of Thin Film Coatings

Kamlendra Vikram[1], Uvaraja Ragavendran[2], Kanak Kalita[1,*], Ranjan Kumar Ghadai[3] and Xiao-Zhi Gao[4]

[1]Department of Mechanical Engineering, Vel Tech Rangarajan Dr. Sagunthala R&D Institute of Science and Technology, Avadi, 600062, India
[2]Department of Electronics and Telecommunication Engineering, MPSTME SVKM'S Narsee Monjee Institute of Management Studies, Shirpur, 425405, India
[3]Department of Mechanical Engineering, Sikkim Manipal Institute of Technology, Sikkim Manipal University, Majhitar, 737136, India
[4]School of Computing, University of Eastern Finland, Kuopio, 70211, Finland
*Corresponding Author: Kanak Kalita. Email: drkanakkalita@veltech.edu.in
Received: 26 August 2020; Accepted: 25 September 2020

Abstract: In this work, diamond-like carbon (DLC) thin film coatings are deposited on silicon substrates by using plasma-enhanced chemical vapour deposition (PECVD) technique. By varying the hydrogen (H_2) flow rate, CH_4–Argon (Ar) flow rate and deposition temperature (T_d) as per a Box-Behnken experimental design (BBD), 15 DLC deposition experiments are carried out. The Young's modulus (E) and the coefficient of friction (COF) for the DLCs are measured. By using a second-order polynomial regression approach, two metamodels are built for E and COF, that establish them as functions of H_2 flow rate, CH_4-Ar flow rate and T_d. A non-dominated sorting genetic algorithm (NSGA-III) is used to obtain a set of Pareto solutions for the multi-objective optimization of E maximization and COF minimization. According to various practical scenarios, evaluation based on distance from average solution (EDAS) approach is used to identify the most feasible solutions out of the Pareto solution set. Confirmation experiments are conducted which shows the efficacy of the polynomial regression—NSGA-III—EDAS hybrid approach. The surface morphology of the DLCs deposited as per the optimal predictions is also studied by using atomic force microscopy.

Keywords: Multi-objective optimization; regression analysis; thin-film coating

1 Introduction

The excellent mechanical, tribological and optical properties of diamond-like carbon (DLC) coatings offer a wide application in the automotive and electronic industries. DLC coating is a mixture of both graphite-like sp2 bond and diamond-like sp3 bonds which shows that the properties of DLCs depend on the number of bonds present within the coatings. DLCs are considered to be the hybrid form of carbon which holds both graphite-like sp2 bond and diamond-like sp3 bonds [1]. It is well known that graphite

(100% sp2) is having a zero-band gap whereas diamond (100% sp3 bond) has a bandgap of 5.5 eV and thus, by the synthesis of DLCs by using different methods the amount of sp3 and sp2 bonds can be altered [2]. Due to the mixture of sp2 and sp3 bonds within the DLC films, it possesses characteristics of both graphite and diamond. The good electrical and electronic properties of DLC are due to the sp2 hybridized carbon whereas, the tribological and mechanical properties are due to the sp3 hybridized carbon [3,4]. DLC films are also used for making surgical equipments, automotive engine parts, magnetic storage discs, micro-electromechanical devices (MEMS), etc.

Various chemical vapour deposition (CVD) techniques are used for the deposition of thin-film coatings and out of all the CVD techniques, plasma-enhanced chemical vapour deposition (PECVD) technique is most widely used for the DLC coating synthesis because of its quality coating at low temperature [5–7]. The different PECVD deposition parameters like gas flow rate, duty cycle, gas composition, deposition temperature, power supply etc. influence the properties of DLC thin films. In recent years, the selection of deposition parameters is a matter of prime concern for the researchers to get the desired properties of the films [8,9]. Singh et al. [10] used a Taguchi technique to find the combination of PECVD deposition parameters like bias voltage (V), bias frequency (f), gas composition, deposition pressure (P) of DLC coatings with PECVD technique to get optimum response parameters, i.e., roughness and hardness. Ghadai et al. [11] used particle swarm optimization (PSO) techniques to optimize the PECVD process parameters to get high hardness of the DLC coating. In an extension to the previous work, Ghadai et al. [12] found that symbolic regression metamodels are superior to traditional polynomial regression metamodels. The symbolic regression metamodels were form-free and thus, were better at modelling the inherent non-linearity in the deposition process. Ghadai et al. [13] also used a genetic algorithm to fine-tune the DLC deposition parameters in APCVD process.

Despite the considerable amount of work done on DLC thin film coatings, only a handful of works are seen on the implementation of advance computational intelligence techniques like multi-objective optimization based on metamodels. This work attempts to address this lacuna by building metamodels that express two different DLC performance parameters (Young's modulus and coefficient of friction) as functions of three DLC deposition process parameters (hydrogen flow rate, CH_4-Argon flow rate and deposition temperature). The metamodels are then deployed in conjunction with the non-dominated sorting genetic algorithm (NSGA-III) for carrying out Pareto optimization. Finally, based on certain scenarios, a multi-criteria decision-making method called EDAS is used to identify the desirable solutions from the Pareto set. Surface morphologies of these optimal designs are studied by using atomic force microscopy.

2 Materials and Methods

2.1 Experimental Procedure

In the work, the synthesis of DLC coatings over silicon (Si) was done by using PECVD deposition technique. To remove the oxide layer, the substrates were dipped into 2% HF solution for 4 min followed by ultrasonic cleaning in deionized water for 10 min. Tab. 1 shows the details of input parameters like hydrogen (H_2) flow rate, CH_4-Argon (Ar) flow rate and temperature for the deposition (T_d) of DLC coatings. The morphological analysis of the DLC coating is done with the help of Innova SPM atomic force microscope. The Young's modulus (E) of the DLC coatings were calculated by using a nano-hardness tester (NHTX-55-0019) of CSM Instruments having Berkovich indentor. The radius of curvature of the indentor (B-I 93) is 20 μm. The indentation was considered at three different locations and the average of that value is considered and the maximum load is taken as 10 mN. The Oliver–Pharr method [14] is applied for the calculation of Young's modulus (E). The nano scratch tests were performed over the coating by using CSM instrument with a sphero-conical diamond indenter (R = 2 μm, SB-A63), by applying a load of 20 mN with a scratch speed of 1 mm/min over a 0.5 mm scratch length.

Table 1: Experimental readings of Young's modulus and coefficient of friction measured at selected BBD sample points

Exp. no.	CH_4-Argon flow rate	H_2 flow rate	Deposition temperature	Young's modulus (Gpa)	Coefficient of friction
1	0.5	40	100	146.80	0.100
2	2	30	80	137.50	0.126
3	1	30	100	178.00	0.087
4	2	30	120	154.00	0.082
5	1	20	120	138.80	0.150
6	0.5	20	100	152.30	0.142
7	1	20	80	128.56	0.110
8	2	40	100	179.20	0.102
9	1	40	80	110.24	0.200
10	0.5	30	120	186.54	0.090
11	1	30	100	166.20	0.130
12	0.5	30	80	106.10	0.160
13	1	40	120	242.00	0.070
14	1	30	100	171.30	0.131
15	2	20	100	146.23	0.180

2.2 Predictive Modeling with Polynomial Regression

In this work, the metamodels for Young's modulus and the coefficient of friction are built by fitting a second-order polynomial regression equation of the following form.

$$\widehat{y_i} = \beta_0 + \beta_1 x_1 + \beta_2 x_2 + \beta_3 x_3 + \beta_4 x_1 x_2 + \beta_5 x_1 x_3 + \beta_6 x_2 x_3 + \beta_7 {x_1}^2 + \beta_8 {x_2}^2 + \beta_9 {x_3}^2 \tag{1}$$

Here $\beta' s$ are the coefficients of regression. These coefficients of regression help in describing the response (y_i) as a function of predictor variables ($x' s$). x_1, x_2 and x_3 represent hydrogen (H_2) flow rate, CH_4-Argon (Ar) flow rate and deposition temperature (T_d) respectively.

Using the Box–Behnken experimental design in Tab. 1, Eq. (1) is fitted based on multiple regression fitting scheme. The difference between the predicted value ($\widehat{y_i}$) and the actual experimental value (y_i) of the response is called the residue [15].

$$\epsilon_i = y_i - \widehat{y_i} \tag{2}$$

$\beta' s$ in Eq. (1) are computed such that the residual sum of squared (RSS) is minimized.

$$RSS = \sum_{i=1}^{n} {\epsilon_i}^2 \tag{3}$$

where n is the number of experimental points in Tab. 1.

2.3 Optimization with NSGA-III

In this work, non-dominated sorting genetic algorithm III (NSGA-III) [16,17] is used for carrying out the Pareto optimization. The multi-objective optimization problem is stated as,

Find $X = (x_1, x_2 \text{ and } x_3)$

which maximizes $Y_1 = f_1(X)$ and minimizes $Y_2 = f_2(X)$ (4)

subject to ${x_1}^l \leq x_1 \leq {x_1}^u$; ${x_2}^l \leq x_2 \leq {x_2}^u$; ${x_3}^l \leq x_3 \leq {x_3}^u$

In Eq. (4), Y_1 and Y_2 are Young's modulus (E) and coefficient of friction (COF) respectively.

NSGA-III is realized in this work by using the following pseudo-code.

START

Define objective functions Y_1 and Y_2

Initiate generation counter $t = 0$

Initiate a random population of n_{pop} individuals

Calculate the fitness of each individual

Conduct non-dominated sorting of individuals

Assign ranks and select parents

Generate child population

Tournament selection

Crossover and mutation

Do

Do for all individuals

Calculate fitness

Conduct non-dominated sorting

Generate Pareto fonts

Determine crowing distance

Loop inside by adding solution to next generation from the first front until n_{pop}

END

Select points on lower front with high crowding distance

Create the next generation

Tournament selection

Crossover and mutation

Until $t = t_{max.}$

Report the Pareto front having P_{nd} non-dominated solutions

END

---

3 Results and Discussion

3.1 Predictive Modeling

Using the training data listed in Tab. 1, second-order polynomial regression metamodels are developed for the prediction of Young's modulus (E) and the coefficient of friction (COF). The coefficients of regression for the metamodels of E and COF are mentioned in Tab. 2. Fig. 1 shows the variation of the predicted values of E and COF for their respective experimental values. It should be noted that closer the values are to the diagonal (identity) line in Fig. 1, better are the estimations of the metamodel. In general, the metamodel for E is seen to have better performance than COF. To further analyze the utility of the two metamodels, the residuals in each case are evaluated against their respective predicted values, as shown in Fig. 2. A random scatter is seen in both cases, which indicates that the residues do not show any trend with the predicted values. Thereby it can be concluded that the metamodels are appropriate as they can quantify the variance in the training data. Further analysis of the residuals is done by plotting their normal probability plots in Fig. 3. No outliers are seen in Fig. 3, which further confirms the efficacy of the metamodels.

Table 2: Regression coefficients for the second-order metamodels

Regression coefficient	Young's modulus	Coefficient of friction
β_0	−72.8926	−2.31E-01
β_1	156.2961	2.66E-02
β_2	−12.7616	1.20E-02
β_3	4.9633	4.71E-03
β_4	0.9127	−1.82E-03
β_5	−1.1282	3.47E-04
β_6	0.1519	−2.13E-04
β_7	−26.6650	−2.83E-03
β_8	−0.0342	1.65E-04
β_9	−0.0338	2.14E-19

3.2 Influence of Process Parameters on the Young's Modulus

Fig. 4 shows the effect of H_2 and CH_4-Ar flow rate on Young's modulus (E) of the DLCs. It is seen that deposition temperature (T_d) has a significant effect on the role that of H_2 and CH_4-Argon flow rate plays on E. For example—at a lesser T_d, the E of the DLCs increase with the increase in CH_4-Argon flow rate but the E decreases with an increase in H_2 flow rate. The trend is the opposite when higher levels of T_d is considered. Similarly, Fig. 5 shows the interactive effect of T_d and CH_4-Ar flow rate on E at various levels of H_2 flow. It is observed that the E increases as the T_d and CH_4-Argon flow rate increases. Fig. 6 shows that the increase in H_2 flow, in general, decreases the E of the DLCs.

3.3 Influence of Process Parameters on the Coefficient of Friction

Fig. 7 shows the effect of H_2 and CH_4-Ar flow rate on the coefficient of friction (COF) of the DLCs. It is seen that the trend of the COF of the DLCs is also significantly affected by the T_d. At low T_d, the increase in H_2 and CH_4-Argon flow rate increases the COF of the DLCs, whereas at higher levels of T_d, the COF decreases with an increase in H_2 flow rate but CH_4-Argon flow rate has a negligible effect on it. In Fig. 8, the trend of COF with T_d and CH_4-Argon flow rate is similar for mid and high level H_2 flow rate but is

significantly different for low H_2 flow rate. At mid and high H_2 flow rate, the COF increases with a decrease in T_d, but is not much affected by variation in CH_4-Argon flow rate. However, as seen in Fig. 9, the behaviour of the COF of the DLCs is similar at all levels of CH_4-Argon flow rate.

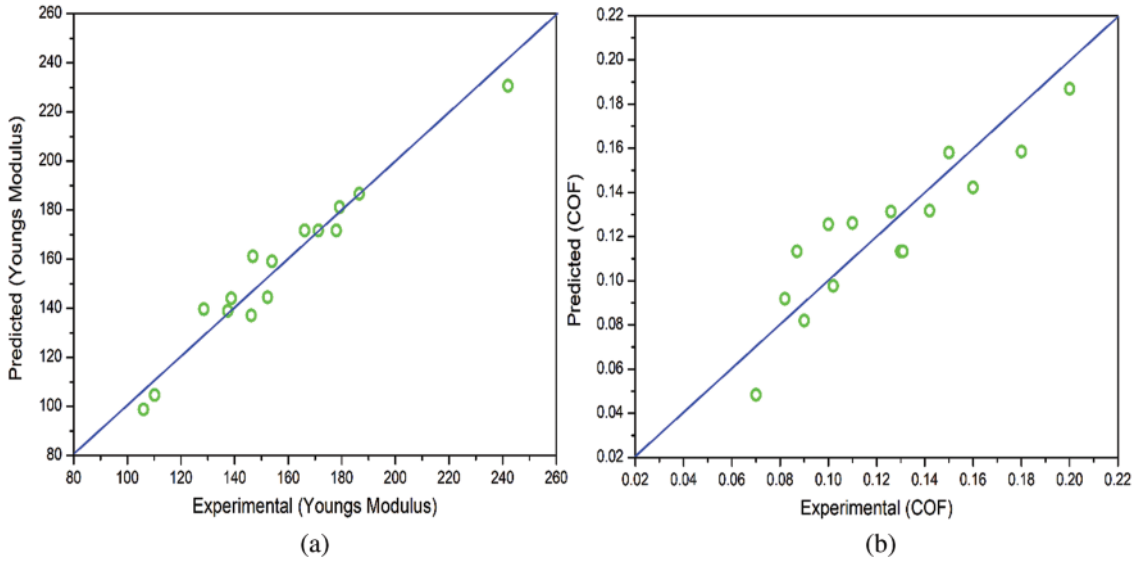

Figure 1: Predicted versus the experimental output responses. (a) Young's modulus, (b) Coefficient of friction

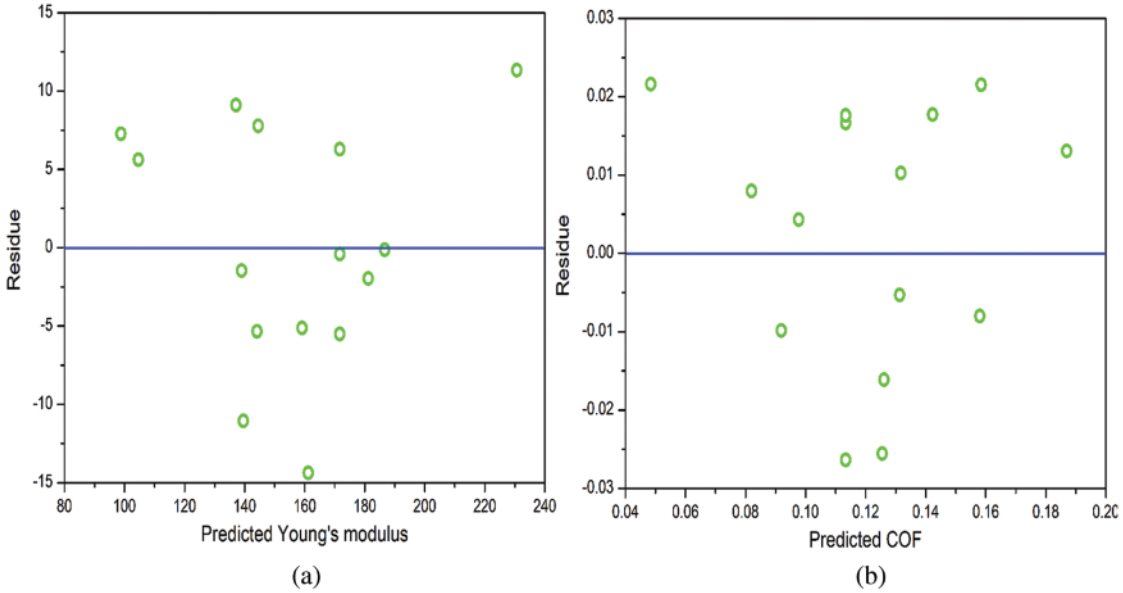

Figure 2: Variation of the residuals with predicted output responses. (a) Young's modulus, (b) Coefficient of friction

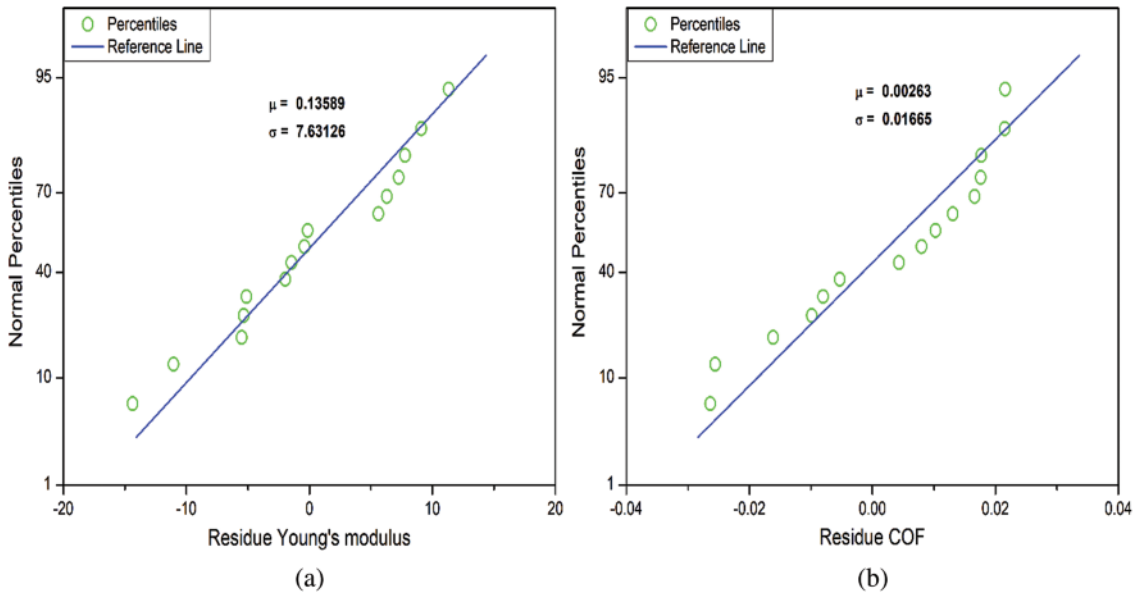

Figure 3: Normal probability plots for the residuals of the metamodels. (a) Young's modulus, (b) Coefficient of friction

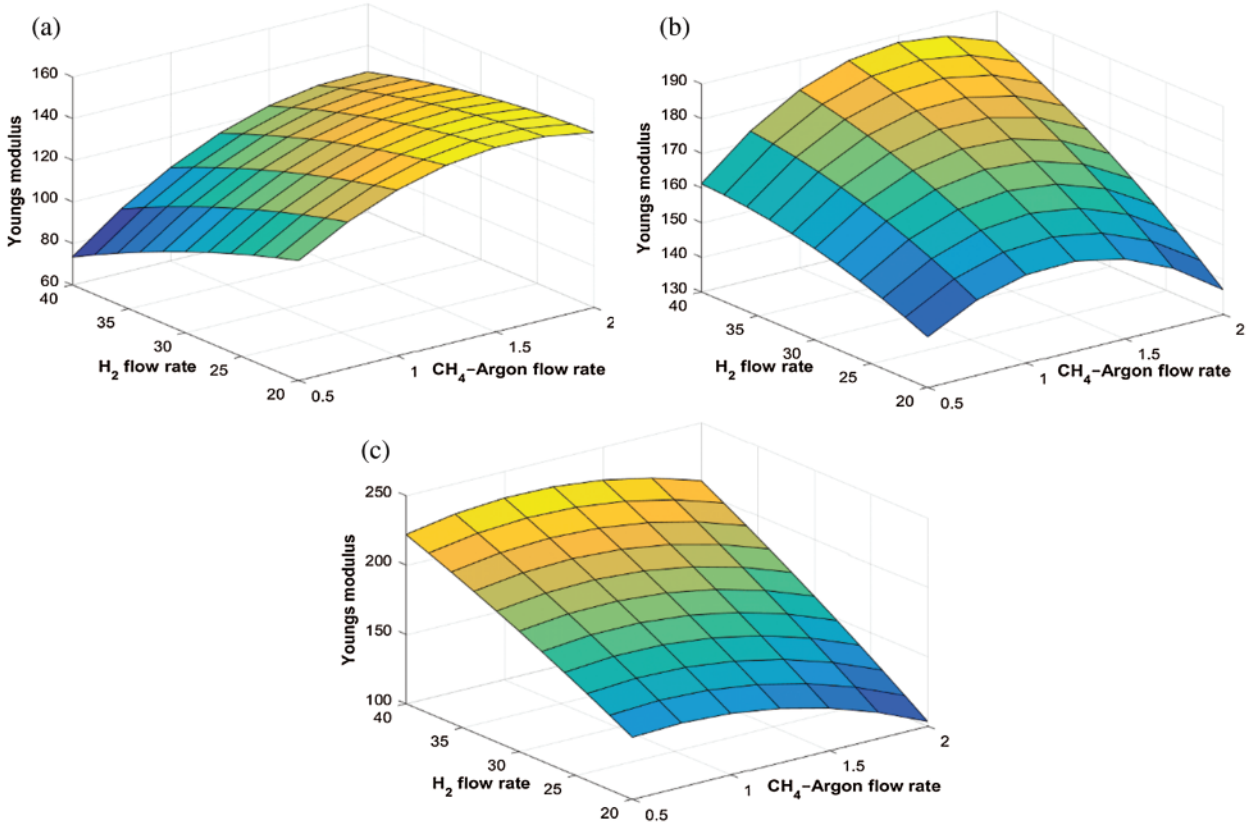

Figure 4: Variation of Young's modulus with $\mathbf{H}_2$ flow rate and CH_4-Argon flow rate at different deposition temperatures. (a) $\mathbf{T}d = 80°C$ (b) $\mathbf{T}d = 100°C$, and (c) $\mathbf{T}d = 120°C$

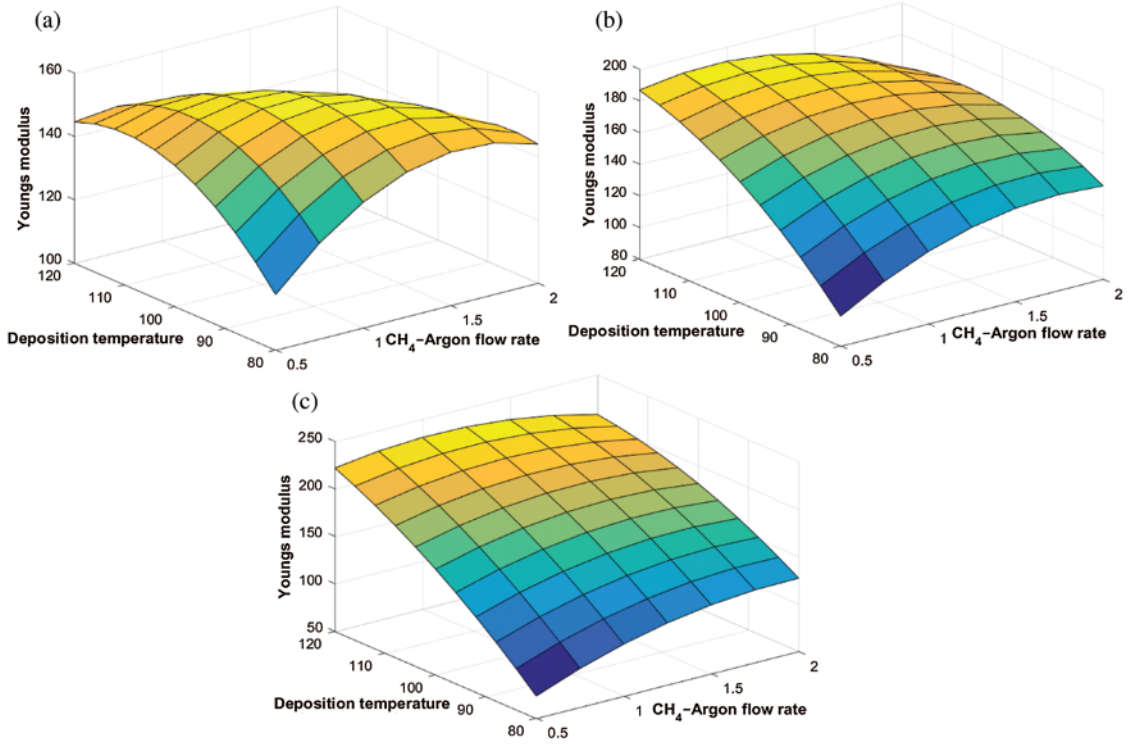

Figure 5: Variation of Young's modulus with deposition temperature and CH_4-Argon flow rate at different H_2 flow rates. (a) 20 sccm, (b) 30 sccm, and (c) 40 sccm

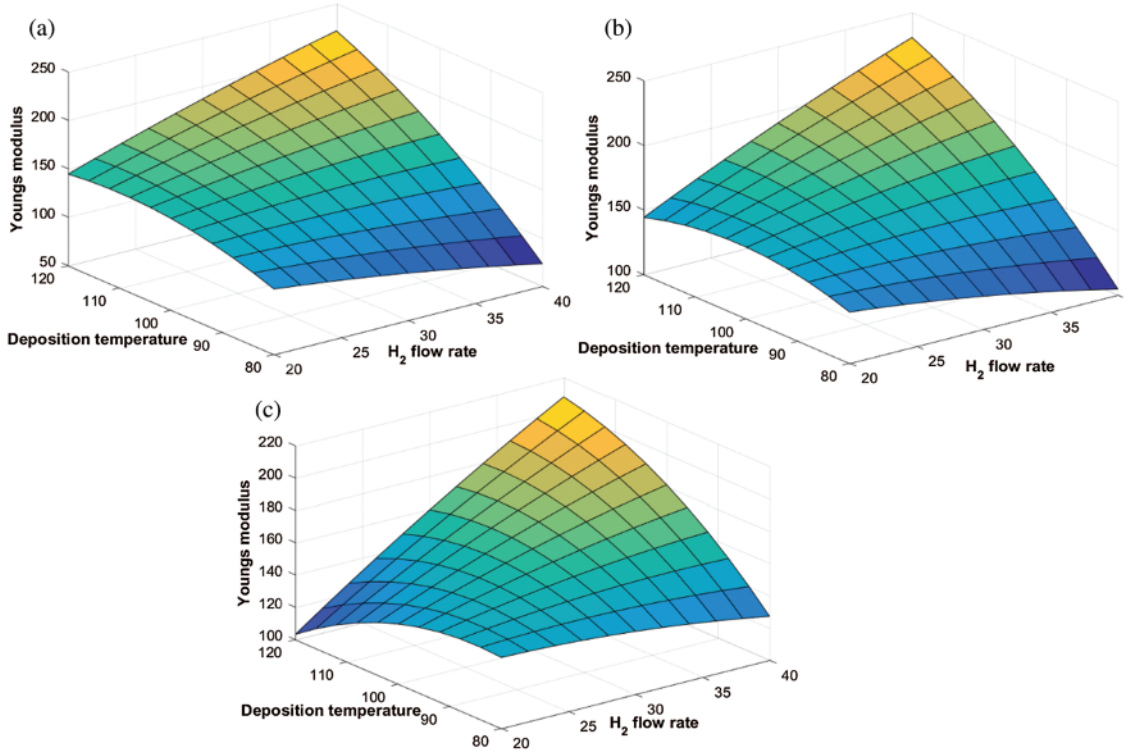

Figure 6: Variation of Young's modulus with deposition temperature and H_2 flow rate at different CH_4-Argon flow rates. (a) 0.5 sccm, (b) 1 sccm, and (c) 2 sccm

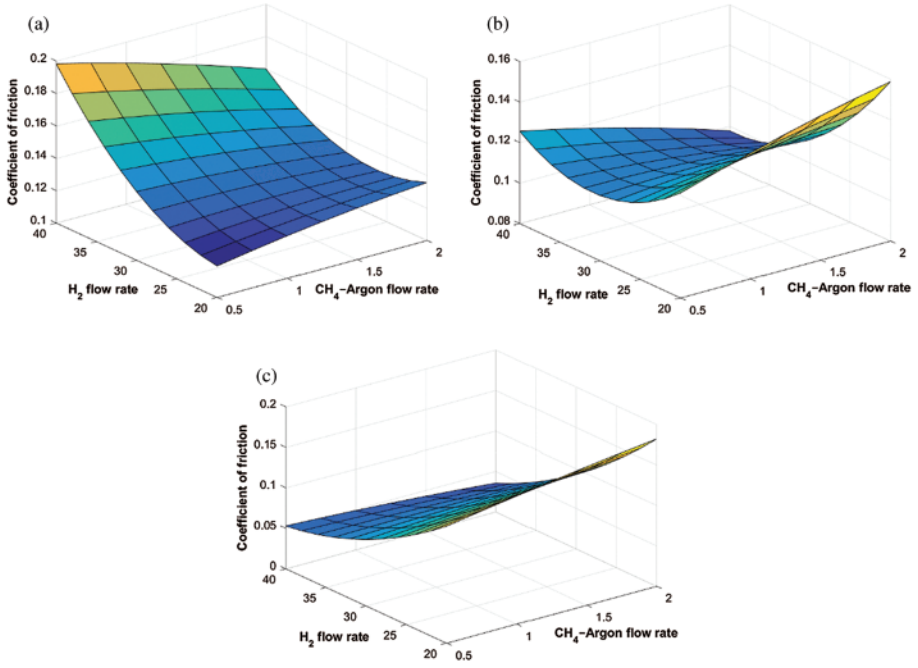

Figure 7: Variation of the coefficient of friction with $\mathbf{H}_2$ flow rate and CH_4-Argon flow rate at different deposition temperatures. (a) $\mathbf{T}d = 80°C$ (b) $\mathbf{T}d = 100°C$ (c) $\mathbf{T}d = 120°C$

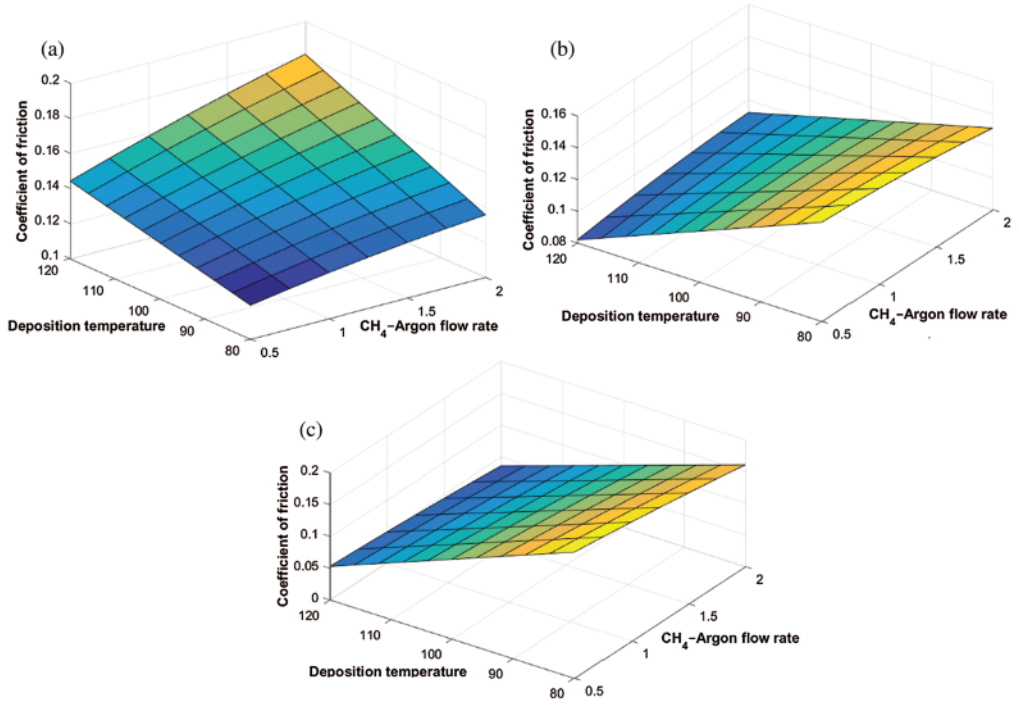

Figure 8: Variation of the coefficient of friction with deposition temperature and CH_4-Argon flow rate at different $\mathbf{H}_2$ flow rates. (a) 20 sccm, (b) 30 sccm, and (c) 40 sccm

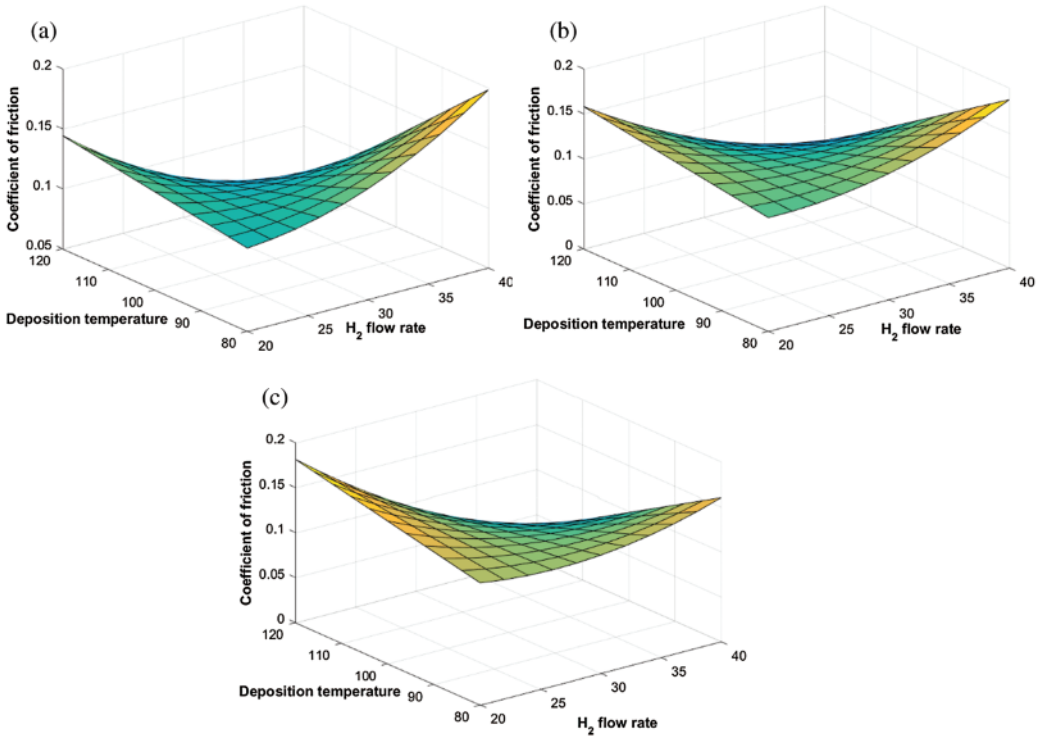

Figure 9: Variation of the coefficient of friction with deposition temperature and H_2 flow rate at different CH_4-Argon flow rates. (a) 0.5 sccm, (b) 1 sccm, and (c) 2 sccm

3.4 Pareto Optimization

Based on the discussion on the effect of the DLC deposition process parameters on Young's modulus and COF in the previous two sections, it is seen that the optimal setting of the two response parameters has conflicting requirements in terms of process parameter settings. Thus, it is not possible to arbitrary decide the optimal parameter combination that would simultaneously maximize the E and minimize the COF. Thus, a Pareto optimization using non-dominated sorting genetic algorithm is carried out and depicted in Fig. 10. The continuous Pareto front in Fig. 10b shows that as the E of the DLCs improve, there is an increase in COF as well. Thus, each solution within the Pareto front in Fig. 10b represents a possible compromise solution to the multi-objective problem. Since it is not possible to arbitrarily draw a particular solution out of the Pareto front to represent a feasible solution, a multi-criteria decision-making approach called EDAS is used to select the most plausible solutions pertaining to certain practical scenarios and are presented in Tab. 3.

3.5 Experimental Confirmation of Optimal Results

Confirmation experiments as per the optimal process parameters are conducted and the experimental values are reported in Tab. 3. The 3-D and 2-D atomic force microscopy (AFM) images of DLC coatings for the validation of optimal point of scenario (A/B/C), (D) and (E) are shown in Figs. 11–13, respectively. The surface roughness (R_a) of the coatings for scenario (A/B/C), (D) and (E) are 15.5 nm, 28 nm, and 32 nm respectively. From the figures, it is observed that small, agglomerated particles are formed for all the cases. The maximum and average particle size for the experimental results for scenario (A/B/C) is 7 nm and 1.5 nm, for scenario (D) the sizes are 15.4 nm and 3.4 nm, for scenario (E) the sizes are 44.2 nm and 7 nm respectively. In all the different scenarios the H_2 flow rate and deposition

temperature are the same, however, the CH_4-Argon flow rate is different. From the experimental results shown in Tab. 3, it is observed that the COF of the DLC coating decreases with an increase in the CH_4-Argon flow rate. From the AFM images, it is observed that the DLC coating having less COF has a smooth surface and result is confirmed from the R_a value. Overall, the confirmation experiment values are seen to be close to the predicted optimal solutions.

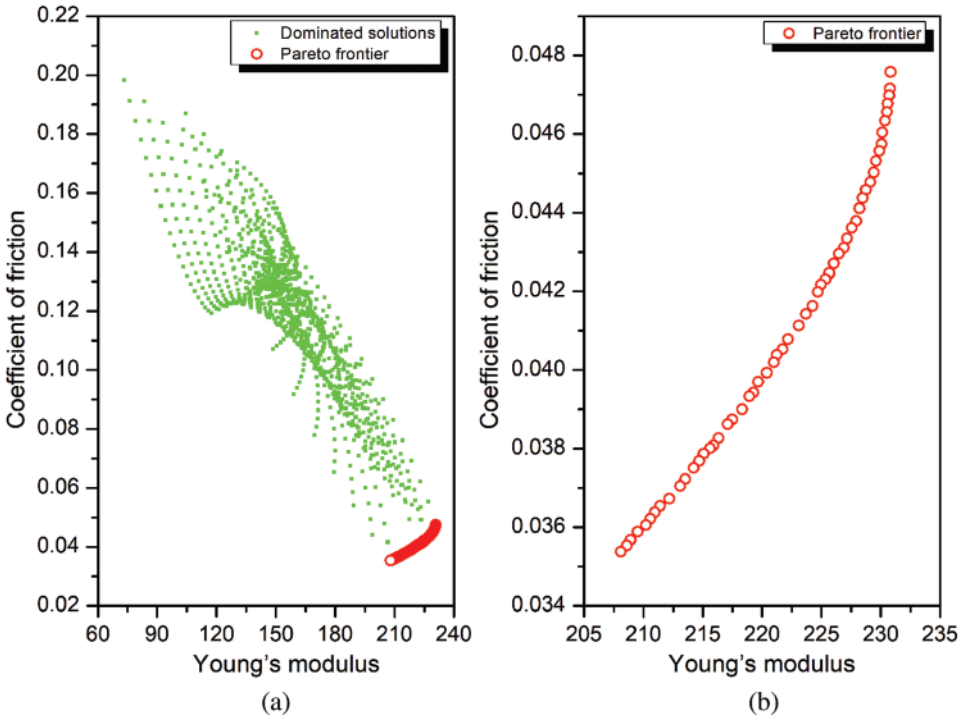

Figure 10: Multi-objective optimization of Young's modulus and COF (a) Dominated and non-dominated solutions, (b) Enlarged view of Pareto frontier

Table 3: EDAS selected optimal solution from the Pareto front

Scenario	W_1(%)[1]	EDAS performance measure	CH_4-Ar flow rate	H_2 flow rate	T_d	E (Gpa)		COF	
						Pred.	Exp.	Pred.	Exp.
A	10	0.97832							
B	25	0.93497	2.00	40	120	208.08595	214	0.03538	0.066
C	50	0.80491							
D	75	0.62844	1.41[2]	40	120	227.92423	212	0.04379	0.08
E	90	0.86518	1.14[3]	40	120	230.71794	219	0.04698	0.094

[1] W_1 is the weight or importance attributed to the criteria Youngs modulus. (100-$\mathbf{W_1}$) is the weight attributed to the criteria COF.
[2] For experiments CH_4-Argon flow rate was considered as 1.5.
[3] For experiments CH_4Argon flow rate was considered as 11.

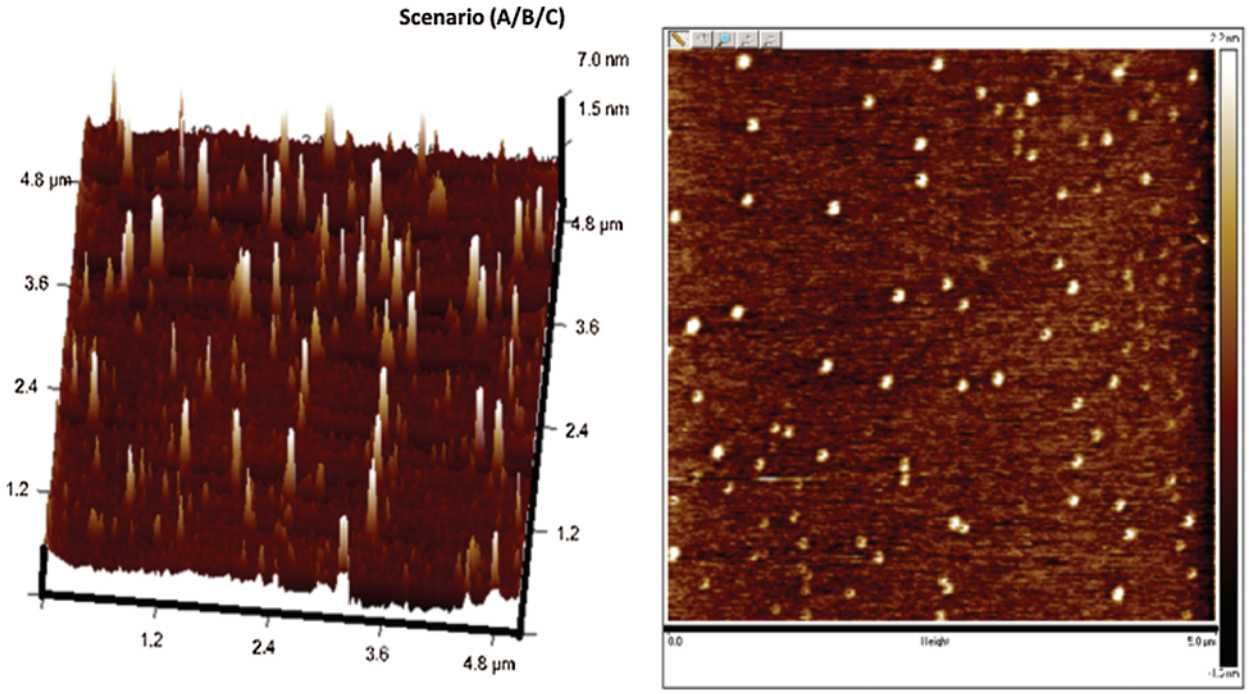

Figure 11: AFM images of deposited DLCs as per scenario A/B/C

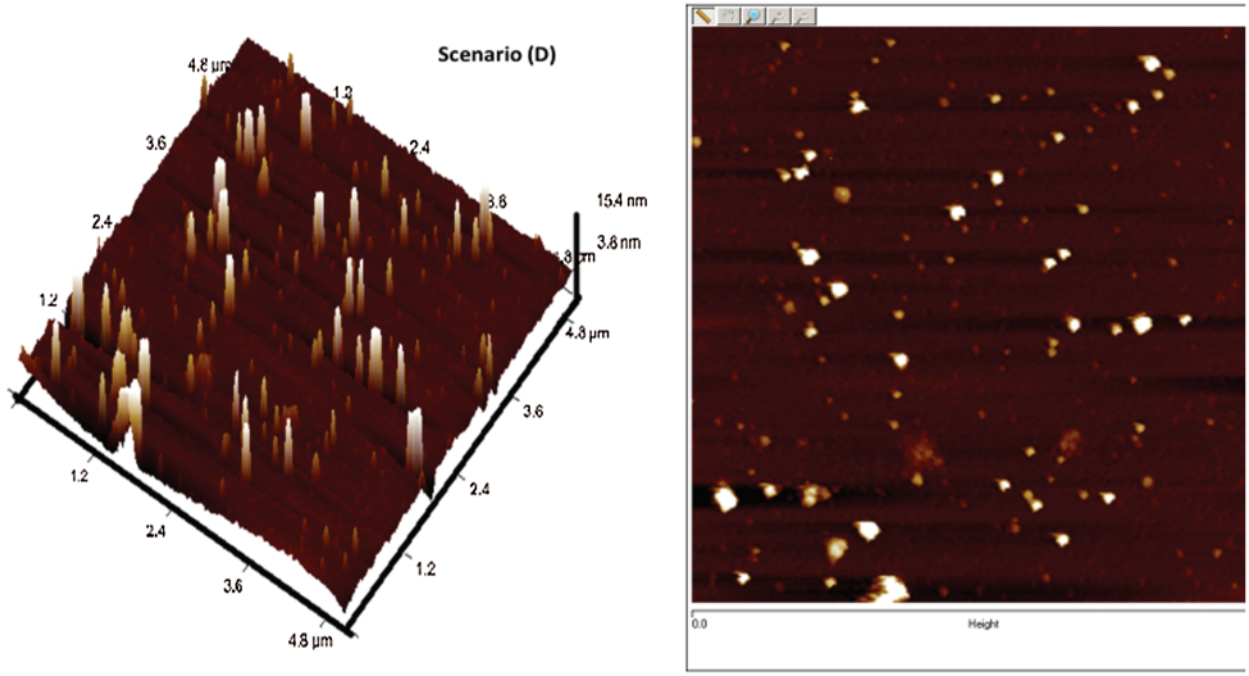

Figure 12: AFM images of deposited DLCs as per scenario D

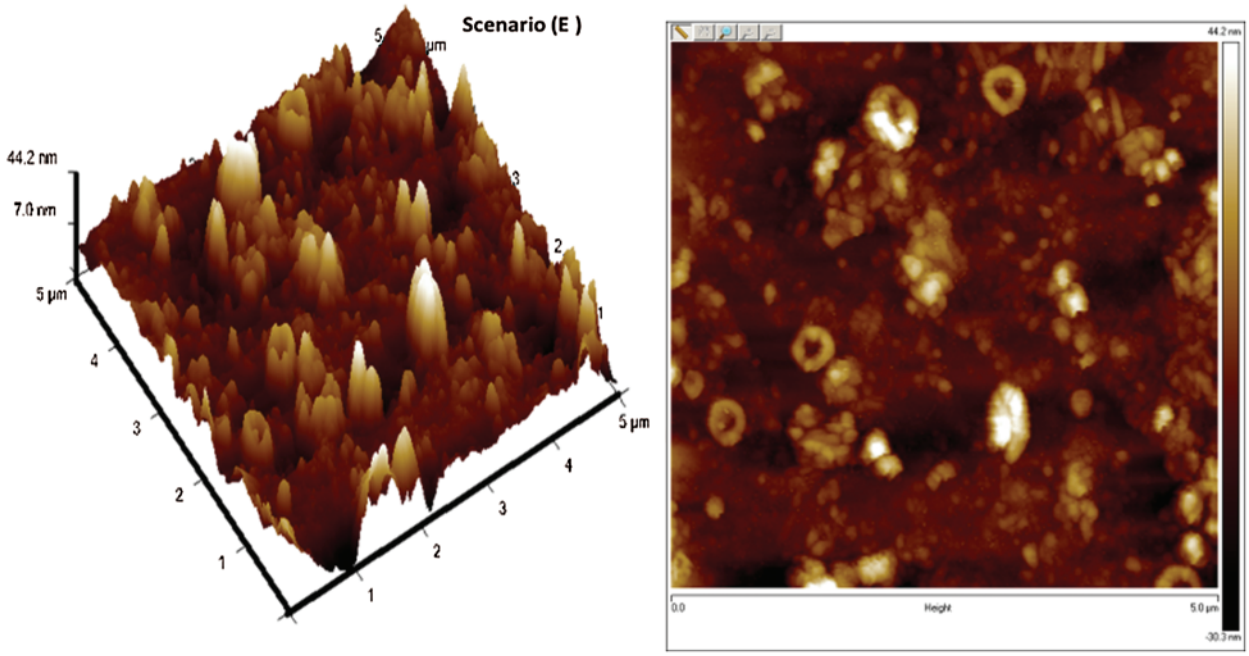

Figure 13: AFM images of deposited DLCs as per scenario E

4 Conclusion

Finding an optimal combination of process parameters that enhances the performance of a process is a realistic goal with tremendous practical implications. In this work, such an effort for optimizing the DLC deposition process parameters is undertaken to suitably enhance Young's modulus and coefficient of friction of DLC thin film coatings. Based on the study the following conclusion are made

- Second-order polynomial regressions can serve as reliable metamodels for DLC process modelling that can be subsequently used for process parameter effect study or in case of optimization scenarios.
- Non-dominated sorting genetic algorithm (NSGA-III) is a viable tool for Pareto optimization of such critical processes. Improvement in Young's modulus of the DLCs was in general accompanied by worsening of the coefficient of friction. Thus, given such conflicting process performance, the Pareto set, as opposed to single-objective solutions, can provide the designer with a lot of flexibility regarding setting the preferred process parameters.
- In general, a higher level of hydrogen flow rate and deposition temperature was found to be suitable in augmenting the young's modulus of the DLCs.
- Confirmation experiments conducted as per the optimal process parameters showed that the polynomial regression—NSGA-III—EDAS approach is reliable and accurate.

Acknowledgement: Authors acknowledge the support of COE, Manipal University in carrying out the characterizations.

Funding Statement: This research was partially funded by TMA Pai University Research Fund, Manipal Group, India (Grant No. 6100/SMIT/R&D/Project/08/2018).

Conflicts of Interest: The authors declare that they have no conflicts of interest to report regarding the present study.

References

[1] J. Robertson, "Diamond-like amorphous carbon," *Materials Science and Engineering: R: Reports*, vol. 37, no. 4, pp. 129–281, 2002.

[2] M. Moseler, P. Gumbsch, C. Casiraghi, A. C. Ferrari and J. Robertson, "The ultrasmoothness of diamond-like carbon surfaces," *Science*, vol. 309, no. 5740, pp. 1545–1548, 2005.

[3] H. Li, T. Xu, C. Wang, J. Chen, H. Zhou *et al.,* "Annealing effect on the structure, mechanical and tribological properties of hydrogenated diamond-like carbon films," *Thin Solid Films*, vol. 515, no. 4, pp. 2153–2160, 2006.

[4] M. Kihel, R. Clergereaux, D. Escaich, M. Calafat, P. Raynaud *et al.,* "Investigations on electrical properties of a-C:H thin films deposited in a microwave multipolar plasma reactor excited at distributed electron cyclotron resonance," *Diamond and Related Materials*, vol. 17, no. 7, pp. 1710–1715, 2008.

[5] R. K. Ghadai, S. Das, D. Kumar, S. C. Mondal and B. P. Swain, "Correlation between structural and mechanical properties of silicon doped DLC thin films," *Diamond and Related Materials*, vol. 82, pp. 25–32, 2018.

[6] A. Muthuraja, S. Naik, D. K. Rajak and C. I. Pruncu, "Experimental investigation on chromium-diamond like carbon (Cr-DLC) coating through plasma enhanced chemical vapour deposition (PECVD) on the nozzle needle surface," *Diamond and Related Materials*, vol. 100, 107588, 2019.

[7] E. J. D. M. Pillaca, M. A. Ramírez, J. G. Bernal, D. C. Lugo and V. J. Trava-Airoldi, "DLC deposition inside of a long tube by using the pulsed-DC PECVD process," *Surface and Coatings Technology*, vol. 359, no. 1, pp. 55–61, 2019.

[8] O. Keles, Y. Taptik, O. L. Eryilmaz, M. Urgen and A. F. Cakir, "Optimization of ARC-PVD TiN coating process parameters by Taguchi technique," *Quality Engineering*, vol. 12, no. 1, pp. 29–36, 1999.

[9] K. J. Clay, S. P. Speakman, N. A. Morrison, N. Tomozeiu, W. I. Milne *et al.,* "Material properties and tribological performance of rf-PECVD deposited DLC coatings," *Diamond and Related Materials*, vol. 7, no. 8, pp. 1100–1107, 1998.

[10] T. P. Singh and V. S. Jatti, "Optimization of the deposition parameters of DLC coatings with the IC-PECVD method," *Particulate Science and Technology*, vol. 33, no. 2, pp. 119–123, 2015.

[11] R. K. Ghadai, K. Kalita, S. C. Mondal and B. P. Swain, "PECVD process parameter optimization: Towards increased hardness of diamond-like carbon thin films," *Materials and Manufacturing Processes*, vol. 33, no. 16, pp. 1905–1913, 2018.

[12] R. K. Ghadai and K. Kalita, "Accurate estimation of DLC thin film hardness using genetic programming," *International Journal of Materials Research*, vol. 11, no. 6, pp. 453–462, 2020.

[13] R. K. Ghadai, K. Kalita, S. C. Mondal and B. P. Swain, "Genetically optimized diamond-like carbon thin film coatings," *Materials and Manufacturing Processes*, vol. 34, no. 13, pp. 1476–1487, 2019.

[14] W. C. Oliver and G. M. Pharr, "An improved technique for determining hardness and elastic modulus using load and displacement sensing indentation experiments," *Journal of Materials Research*, vol. 7, no. 6, pp. 1564–1583, 1992.

[15] K. Kalita, P. Dey and S. Haldar, "Search for accurate RSM metamodels for structural engineering," *Journal of Reinforced Plastics and Composites*, vol. 38, no. 21, pp. 995–1013, 2019.

[16] K. Deb and H. Jain, "An evolutionary many-objective optimization algorithm using reference-point-based nondominated sorting approach part I: Solving problems with box constraints," *IEEE Transactions on Evolutionary Computation*, vol. 18, no. 4, pp. 577–601, 2014.

[17] N. Ganesh, R. K. Ghadai, A. K. Bhoi, K. Kalita and X. Z. Gao, "An intelligent predictive model-based multi-response optimization of EDM process," *Computer Modeling in Engineering & Sciences*, vol. 124, no. 2, pp. 459–476, 2020.